AFFDL-TR-68-150

A REFINED QUADRILATERAL ELEMENT FOR ANALYSIS OF PLATE BENDING

Ray W. Clough*
University of California, Berkeley

Carlos A. Felippa**
Boeing Airplane Company, Renton

The formulation of a fully compatible general quadrilateral plate bending element is described. The element is assembled from four partially constrained linear curvature compatible triangles, arranged so that no mid-side nodes occur on the external edges of the quadrilateral; thus, the resulting element has only 12 degrees of freedom. Also described is a simple shear distortion mechanism which may be incorporated into the element without changing its basic structure. Results are presented for static analyses with and without shear distortion, and for plate vibration and plate buckling studies, all performed with this quadrilateral element. It is concluded that this is the most efficient general bending element yet devised.

*Professor of Civil Engineering
**Research Engineer

SECTION I

INTRODUCTION

HISTORICAL BACKGROUND

The finite element method can be considered as the most powerful and versatile discretization technique presently available for the numerical solution of complex structural problems using digital computers. The method was developed originally as an application of standard structural analysis procedures to a physically discretized approximation of the actual system; the concept has been extensively described elsewhere (References 1, 2, 3, and 4) and will not be detailed here. During the past few years, study of the mathematical foundations of the method (References 5, 6, 7, and 8) as well as its application to a wider class of field problems (Reference 4) has greatly clarified the basic requirements for its effective formulation.

The application of the finite element method to plate bending problems dates from the late 1950's. The first successful results were published in 1960 (References 9, 10, and 11), but were obtained using rectangular elements, none of which satisfied the requirements listed in the following section. The construction of adequate displacement expansions for the more versatile triangular and quadrilateral shapes was not achieved until 1965, most of these results being presented at the 1st Air Force Institute of Technology (AFIT) Conference (References 12, 13, and 14). By this time, basic guides for the selection of suitable element deformation patterns had been set forth empirically (Reference 15) and later rigorously proved (References 7, and 8). Most of the early developments in plate bending analysis by finite elements are summarized in Reference 12. During the three years since the 1st AFIT Conference, a considerable number of publications has been devoted to general plate bending elements. Several displacement-assumed models with various degrees of refinement have been proposed (References 16, 17, 18, 19, 20, 21, and 22) as well as elements for analyses based on equilibrium (References 14, 23, and 24), mixed (References 25, 26, 27, 28, and 29) and "hybrid" (References 30, and 31) variational principles.

In view of this long list of alternatives, it is important to consider which alternative provides the best balance in practical usage, taking into consideration factors such as simplicity of formulation, versatility of application, reliability, computational effort, and accuracy. The purpose of this paper is to describe a general quadrilateral element, formed as an assemblage of triangular elements, which is believed to be one of the most efficient

mesh units for both plate and thin shell applications. The quadrilateral element is designated Q-19 to identify it as a quadrilateral with 19 basic degrees of freedom. (It is reduced to 12 degrees of freedom before incorporating into an element assemblage.) The triangular elements of which it is formed are designated LCCT-11, meaning Linear Curvature Compatible Triangle with 11 degrees of freedom. The 9-degree of freedom version of this element (LCCT-9) is the same as that designated HCT in Reference 12.

The element stiffness derivation is outlined completely, after the basic requirements and limitations imposed on the assumed displacement expansions are summarized. Then results obtained in various static, dynamic, and buckling analyses are presented to demonstrate the effectiveness of the element.

DISPLACEMENT ASSUMPTION REQUIREMENTS

The transverse displacement w(x,y) is the sole primary variable required in the formulation of the total potential energy of a plate element. The set of assumed displacement patterns in each element should belong to the admissible class of functions satisfying the following requirements:

(1) Compatibility: (a) The assumed w(x,y) must be continuous and have continuous first derivatives inside each element; (b) w(x,y) and its normal derivatives $\partial w/\partial n$ (the normal slope) must be uniquely specified along any element interface S (where n is normal to S) by nodal displacement selected on S.

(2) Completeness: All rigid body displacement states and uniform strain (constant curvature) states must be included in the expansion. In other words, the six terms $1,x,y,x^2,xy,y^2$ (or their equivalent in other coordinate systems) must be included in the set of element displacement modes.

If these requirements are met, the finite element analysis is a special form of the classical Rayleigh-Ritz procedure (Reference 5) in which the nodal displacements are taken as generalized coordinates. For a stable elastic material, it follows from the positive definite character of the total potential energy functional that a sequence of finite element solutions obtained by a mesh subdivision process provides a minimizing sequence for the strain energy. Using Sobolev's inclusion theorem (Reference 32), it can be shown that the transverse displacements converge uniformly whereas slopes, curvatures and bending moments converge in the mean. (If the exact solution is sufficiently smooth, rotations and curvatures also converge uniformly.)

The compatibility requirement is not actually necessary for strain energy convergence. "Non-conforming" elements which violate slope continuity between corners have been used extensively and often with good results (References 5, 10, 11, 12, 13, and 24). If any group of non-conforming elements can represent rigid body and constant curvature states exactly, the finite element solutions will converge to the true value of strain energy (Reference 7), though not necessarily in monotonic form. Although their derivation is simpler, the use of non-conforming elements in general purpose programs has certain disadvantages: (a) energy convergence depends on the mesh subdivision pattern (Reference 13), (b) curvatures and bending moments may not converge even if the strain energy does, and (c) no error control is available.

CONSTRUCTION OF DISPLACEMENT EXPANSIONS

In considering the selection of transverse displacement patterns for general polygonal flat plate elements, it is convenient to distinguish between two classes:

1. Class C^2: the assumed w(x,y) has continuous second derivatives (curvatures) at the element corners (inside the element). Example: single polynomial expansions.

2. Class C^1: w(x,y) may have discontinuous corner curvatures.

The generation of plate elements using C^2 expansions is severely restricted by the following limitation principle (which is proved in Reference 18):

To construct a complete and compatible C^2 plate bending expansion, a minimum of

6 degrees of freedom ($w, w_x, w_y, w_{xx}, w_{xy}$ and w_{yy}) are required at each non-right angled corner, and

4 degrees of freedom (w, w_x, w_y, w_{xy}, where x-y are taken along the adjacent sides) are required at each right-angled corner.

If less degrees of freedom are selected and full compatibility is enforced, completeness is lost and the finite element analysis does not converge. It follows that at least 18 degrees of freedom are required for a general triangle, 24 for an arbitrary quadrilateral and 16 for a rectangle. When polynomial expansions are used, at least a quintic (which provides 21 generalized coordinates) is necessary for a C^2 expansion over a triangle (References 18 and 19.)

The use of C^1 expansions provides more flexibility in the selection of displacement functions, and is essential for generating compatible, complete elements with only three degrees of freedom (w,w_x,w_y) per corner. Two construction methods have been used with success:

(1) C^1 spline fit of several polynomial subexpansions assumed over triangular subregions (References 12, 14 and 20). (The element described in this paper fits into this category.)

(2) Correction of single polynomial expansions with rational functions exhibiting curvature singularities at the corners (References 13 and 20).

Another limitation principle concerning the construction of curved side plate elements is given in Reference 8.

SECTION II

DERIVATION OF THE ELEMENT STIFFNESS MATRICES

STIFFNESS OF THE LCCT-12 ELEMENT

Triangle Geometry

The geometry of an arbitrary triangular element can be expressed in a Cartesian coordinate system by its nodal coordinates or its projected dimensions, as shown in Figure 1a, or alternatively by its intrinsic dimensions as defined in Figure 1b. If j and k denote the first and second cyclic permutations of i = 1,2,3 (i.e., j = 2,3,1 and k = 3,1,2), the projected dimensions may be expressed

$$a_i = x_k - x_j \quad ; \quad b_i = y_j - y_k \tag{1}$$

Also the intrinsic dimensions may be defined in terms of the projected dimensions, one of the more important relationships being

$$d_i = -(a_i a_k + b_i b_k) / L_i \tag{2}$$

The analysis of the stiffness properties of a triangular element is greatly simplified by the use of triangular (natural) coordinates. The triangular coordinates $\zeta_1, \zeta_2, \zeta_3$ of any point "P" in the triangle may be defined either as the ratios of the areas A_i of the sub-triangles subtended by that point to the total area A of the triangle, or as the ratios of the normal distances n_i to the heights H_i; i.e.

$$\zeta_i = \frac{A_i}{A} = \frac{n_i}{H_i} \tag{3}$$

as shown in Figure 2. It should be noted that the triangular coordinates are related by the constraining condition $\zeta_1 + \zeta_2 + \zeta_3 = 1$.

The relationships between Cartesian and triangular coordinates may be expressed as follows

$$\begin{bmatrix} 1 \\ x \\ y \end{bmatrix} = \begin{bmatrix} 1 & 1 & 1 \\ x_1 & x_2 & x_3 \\ y_1 & y_2 & y_3 \end{bmatrix} \begin{bmatrix} \zeta_1 \\ \zeta_2 \\ \zeta_3 \end{bmatrix} \tag{4}$$

or by inversion:

$$\begin{bmatrix} \zeta_1 \\ \zeta_2 \\ \zeta_3 \end{bmatrix} = \frac{1}{2A} \begin{bmatrix} 2A_{23} & b_1 & a_1 \\ 2A_{31} & b_2 & a_2 \\ 2A_{12} & b_3 & a_3 \end{bmatrix} \begin{bmatrix} 1 \\ x \\ y \end{bmatrix} \tag{5}$$

in which $2A_{ij} = x_i y_j - x_j y_i$. From Equation 5, the following important differential relationships between the coordinate systems may be noted:

$$\frac{\partial \zeta_i}{\partial x} = \frac{b_i}{2A} \quad ; \quad \frac{\partial \zeta_i}{\partial y} = \frac{a_i}{2A} \tag{6}$$

Subelement Geometry

It was stated in the Introduction that it is impossible to derive a fully compatible triangular plate bending element using only a single cubic displacement expansion. To obtain a compatible system, the basic element has been divided into three subelements, as shown in Figure 3a in which the internal point "O" is the centroid of the element area, and the subtriangles are numbered to correspond with the opposite corner number. The geometric relationships discussed above apply to each of the subtriangles if its three corners are renumbered 1-2-3, with 3 being taken as the internal point. The subtriangle number is then identified in the algebraic expressions by means of a superscript. The renumbering scheme for Subelement 1 is shown in Figure 3b.

Displacement Interpolation Functions

The nodal displacement degrees of freedom which are to be considered in the stiffness matrix of the complete element also are shown in Figure 3a. These include the transverse displacements of each corner, w_i, the rotations at each corner about the x and y axes, θ_{xi} and θ_{yi}, as well as the rotation at the three mid-side nodes about an axis parallel to the side, θ_4, θ_5 and θ_6. In order to develop displacement patterns for the complete triangle, displacement interpolation functions were assumed independently for each subtriangle.

The displacement interpolation functions for each subelement express the relationship between the displacements $w^{(i)}$ within the element and the ten displacement components of its nodal points $r^{(i)}$, as follows:

$$w^{(i)} = \phi^{(i)} r^{(i)} \tag{7}$$

As may be noted in Figure 3b, the nodal displacement vector for subelement 1 is:

$$r^{(1)T} = \left[w_2 \; \theta_{x2} \; \theta_{y2} \; w_3 \; \theta_{x3} \; \theta_{y3} \; w_o \; \theta_{xo} \; \theta_{yo} \; \theta_5 \right] \tag{8}$$

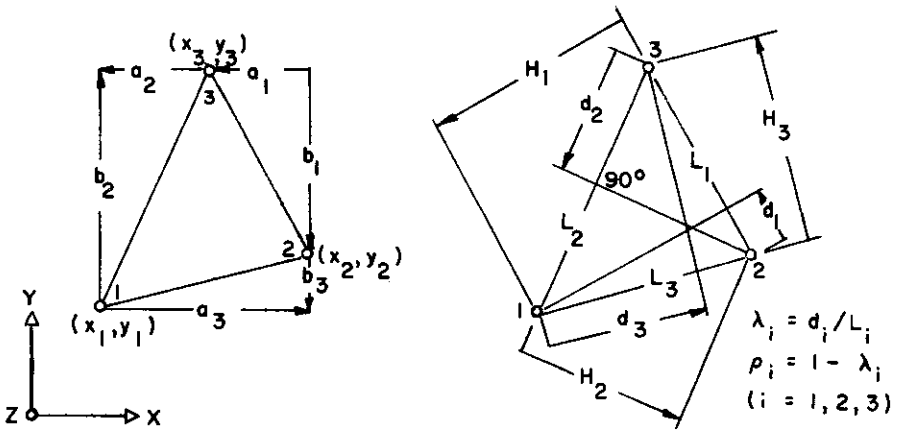

(a) X-Y Projected Dimensions (b) Intrinsic Dimensions

Figure 1. Dimensions of Arbitrary Triangular Element

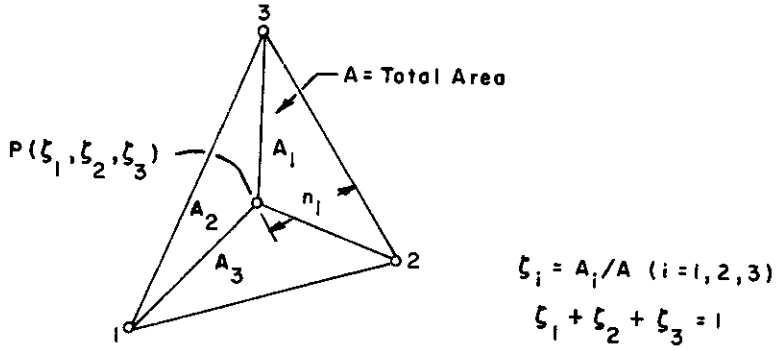

Figure 2. Triangular Coordinate System

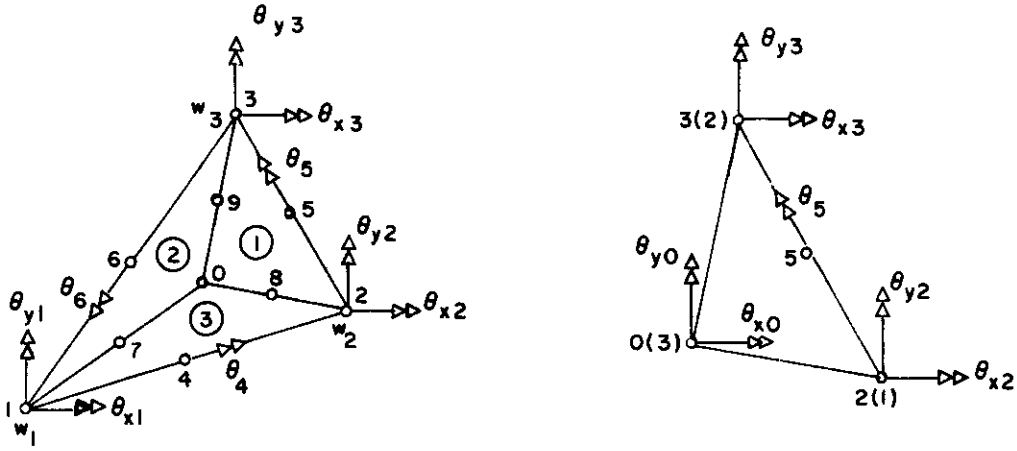

(a) Element Assembly (b) Subelement Nodal System

Figure 3. Assembly of the LCCT-12 Plate Bending Element

The set of 10 cubic interpolation functions for Subelement 1 may be expressed in triangular coordinates as follows:

$$\phi^{(1)T} = \begin{bmatrix} \zeta_1^2(3-2\zeta_1) + 6\mu_3^{(1)}\zeta_1\zeta_2\zeta_3 \\ \zeta_1^2(b_3^{(1)}\zeta_2 - b_2^{(1)}\zeta_3) + (b_3^{(1)}\mu_3^{(1)} - b_1^{(1)})\zeta_1\zeta_2\zeta_3 \\ \zeta_1^2(a_3^{(1)}\zeta_2 - a_2^{(1)}\zeta_3) + (a_3^{(1)}\mu_3^{(1)} - a_1^{(1)})\zeta_1\zeta_2\zeta_3 \\ \zeta_2^2(3-2\zeta_2) + 6\lambda_3^{(1)}\zeta_1\zeta_2\zeta_3 \\ \zeta_2^2(b_1^{(1)}\zeta_3 - b_3^{(1)}\zeta_1) + (b_2^{(1)} - b_3^{(1)}\lambda_3^{(1)})\zeta_1\zeta_2\zeta_3 \\ \zeta_2^2(a_1^{(1)}\zeta_3 - a_3^{(1)}\zeta_1) + (a_2^{(1)} - a_3^{(1)}\lambda_3^{(1)})\zeta_1\zeta_2\zeta_3 \\ \zeta_3^2(3-2\zeta_3) \\ \zeta_3^2(b_2^{(1)}\zeta_1 - b_1^{(1)}\zeta_2) \\ \zeta_3^2(a_2^{(1)}\zeta_1 - a_1^{(1)}\zeta_2) \\ 4H_3^{(1)}\zeta_1\zeta_2\zeta_3 \end{bmatrix} \tag{9}$$

where the subscripts correspond to the renumbered nodes of the subelement. With this convention, the interpolation functions for subelements 2 and 3 are the same as Equation 9, except with appropriately changed superscripts. It should be noted, however, that the nodal displacements in Equation 8 are identified by node numbers defined for the complete element assembly.

Now if the vector $\bar{r}$ of all nodal displacements of the complete element assembly are written in the sequence

$$\begin{aligned} \bar{r}^T &= \left[\, w_1\ \theta_{x1}\ \theta_{y1}\ w_2\ \theta_{x2}\ \theta_{y2}\ w_3\ \theta_{x3}\ \theta_{y3}\ \theta_4\ \theta_5\ \theta_6 \,\vdots\, w_0\ \theta_{x0}\ \theta_{y0} \,\right] \\ &= \left[\, r^T \,\vdots\, r_0^T \,\right] \end{aligned} \tag{10}$$

the displacements in subelement 1 can be expressed

$$w^{(1)} = \bar{\phi}^{(1)}\bar{r} = \left[\, \phi_e^{(1)} \,\vdots\, \phi_0^{(1)} \,\right] \begin{bmatrix} r \\ \hline r_0 \end{bmatrix} \tag{11}$$

where $\bar{\phi}^{(1)}$ is similar to Equation 9, but expanded with 5 zeros to account for the nodal displacements not associated with Element 1, and with appropriate rearrangement of terms. The submatrices $\phi_e^{(1)}$ and $\phi_o^{(1)}$ represent the interpolation functions for the external and internal nodal displacements respectively.

Expressing the displacements in the other subelements similarly, the complete system of displacements can be written:

$$\begin{bmatrix} w^{(1)} \\ w^{(2)} \\ w^{(3)} \end{bmatrix} = \left[\begin{array}{c|c} \phi_e^{(1)} & \phi_o^{(1)} \\ \phi_e^{(2)} & \phi_o^{(2)} \\ \phi_e^{(3)} & \phi_o^{(3)} \end{array}\right] \left[\begin{array}{c} - \\ \frac{r}{r_o} \\ - \end{array}\right] \tag{12}$$

Establishing Internal Compatibility

Equation 12 is an expression of the cubic displacement patterns developed in the three subelements. Because of the common displacements imposed at the nodes, the transverse displacements of two adjacent elements are identical along their juncture line. However, their normal slopes differ between the nodes; hence, Equation 12 does not represent an internally compatible displacement field. To establish slope compatibility along the internal edges of the subelements, additional nodes 7, 8, and 9 were located at the mid-points of these edges, as shown in Figure 3a. The normal slope was computed at each of these nodes in each subelement, for example

$$\left(\frac{\partial w^{(1)}}{\partial n}\right)_7 \equiv \theta_7^{(1)} = \left[\begin{array}{c|c} b_7^{(1)} & b_{70}^{(1)} \end{array}\right] \left[\begin{array}{c} - \\ \frac{r}{r_o} \\ - \end{array}\right] \tag{13}$$

where $b_7^{(1)}$ is $\dfrac{\partial \phi_e}{\partial n}$ and $b_{70}^{(1)}$ is $\dfrac{\partial \phi_o}{\partial n}$ both evaluated at node 7. Similar expressions can be developed for each nodal slope in each subelement. To maintain internal slope compatibility, it is necessary to match the nodal slopes in adjacent subelements, i.e., $\theta_7^{(1)} = -\theta_7^{(3)}$, etc. (where the negative sign results from the convention that the positive normal is directed outward), or stating all three compatibility requirements together:

$$\begin{bmatrix} \theta_7^{(1)} \\ \theta_8^{(2)} \\ \theta_9^{(3)} \end{bmatrix} + \begin{bmatrix} \theta_7^{(3)} \\ \theta_8^{(1)} \\ \theta_9^{(2)} \end{bmatrix} = \left[\begin{array}{c|c} (b_7^{(1)} + b_7^{(3)}) & (b_{70}^{(1)} + b_{70}^{(3)}) \\ (b_8^{(2)} + b_8^{(1)}) & (b_{80}^{(2)} + b_{80}^{(1)}) \\ (b_9^{(3)} + b_9^{(2)}) & (b_{90}^{(3)} + b_{90}^{(2)}) \end{array}\right] \left[\begin{array}{c} - \\ \frac{r}{r_o} \\ - \end{array}\right] = \begin{bmatrix} 0 \\ 0 \\ 0 \end{bmatrix} \tag{14}$$

Equation 14 may be expressed symbolically as follows:

$$\left[\mathbf{B} \;\vdots\; \mathbf{B}_o\right]\left[\frac{\mathbf{r}}{\mathbf{r}_o}\right] = \mathbf{0} \tag{15}$$

Now the values of $\mathbf{r}_o$ which will satisfy these compatibility conditions may be computed from Equation 15; i.e.

$$\mathbf{r}_o = -\mathbf{B}_o^{-1}\,\mathbf{B}\,\mathbf{r} \equiv \mathbf{L}\,\mathbf{r} \tag{16}$$

Finally, introducing the compatibility constraint of Equation 16 into Equation 12, the fully compatible displacement field in the three subelements becomes:

$$\begin{bmatrix} w^{(1)} \\ w^{(2)} \\ w^{(3)} \end{bmatrix} = \left(\begin{bmatrix} \phi_e^{(1)} \\ \phi_e^{(2)} \\ \phi_e^{(3)} \end{bmatrix} + \begin{bmatrix} \phi_o^{(1)} \\ \phi_o^{(2)} \\ \phi_o^{(3)} \end{bmatrix} \mathbf{L} \right) \mathbf{r} \equiv \begin{bmatrix} \hat{\phi}^{(1)} \\ \hat{\phi}^{(2)} \\ \hat{\phi}^{(3)} \end{bmatrix} \mathbf{r} \tag{17}$$

Although it is straightforward in concept, the derivation of the compatible interpolation functions of Equation 17 involves long algebraic manipulations and is a tedious operation. Explicit expressions for these functions are presented in the Appendix for the convenience of the reader.

Internal Curvature Field

In order to define the stiffness matrix corresponding with the derived displacement field, it is necessary to establish the curvatures within the subelements. The most convenient means of defining the curvature distribution is by means of appropriate interpolation functions; in the present case where the assumed displacement functions are cubic, it is important to note that the curvature must vary linearly within each subelement. Thus, the curvature field can be expressed as the product of linear interpolation functions multiplied by curvature values defined at the corner nodes.

Within any subelement "i," the curvature $\chi^{(i)}$ can be obtained by differentiation of the displacement field, thus

$$\chi^{(i)} \equiv \begin{bmatrix} w_{xx}^{(i)} \\ w_{yy}^{(i)} \\ 2w_{xy}^{(i)} \end{bmatrix} = \mathbf{T}^{(i)}\mathbf{r} \tag{18}$$

where

$$T^{(i)} \equiv \begin{bmatrix} \dfrac{\partial^2 \hat{\phi}^{(i)}}{\partial x^2} \\ \dfrac{\partial^2 \hat{\phi}^{(i)}}{\partial y^2} \\ 2\dfrac{\partial^2 \hat{\phi}^{(i)}}{\partial x\, \partial y} \end{bmatrix} \tag{19}$$

Now the nodal values of the curvatures in subelement "i" may be determined by evaluating $T^{(i)}$ at corner points; thus, if the nodal curvatures are designated $\chi_n^{(i)}$ and the nodal values of $T^{(i)}$ are $T_n^{(i)}$ the relationship may be expressed

$$\chi_n^{(i)} = T_n^{(i)} r \tag{20}$$

in which, for example,

$$\chi_n^{(i)T} = \begin{bmatrix} w_{xx2}^{(i)} & w_{xx3}^{(i)} & w_{xxo}^{(i)} & w_{yy2}^{(i)} & w_{yy3}^{(i)} & w_{yyo}^{(i)} & 2w_{xy2}^{(i)} & 2w_{xy3}^{(i)} & 2w_{xyo}^{(i)} \end{bmatrix} \tag{21}$$

The linear curvature variation within the subelement can now be expressed by means of the linear interpolation functions ϕ_x as follows:

$$\chi^{(i)} = \begin{bmatrix} \phi_x & 0 & 0 \\ 0 & \phi_x & 0 \\ 0 & 0 & \phi_x \end{bmatrix} \chi_n^{(i)} \equiv \overline{\phi_x}\, \chi_n^{(i)} \tag{22}$$

where the linear interpolation functions are merely the three triangular coordinates:

$$\phi_x = \begin{bmatrix} \zeta_1 & \zeta_2 & \zeta_3 \end{bmatrix} \tag{23}$$

It is of interest to note that the curvatures in the three subelements are identical at the nodal point "O"; thus, these quantities need be evaluated only once.

Element Stiffness

The strain energy due to bending of the subelement may be obtained by integrating the product of the moments and the curvatures over the area of the element, i.e.

$$U^{(i)} = \frac{1}{2} \int_A m^{(i)^T} \chi^{(i)} dA \tag{24}$$

where the internal moments are given by

$$m^{(i)} \equiv \begin{bmatrix} m_{xx}^{(i)} \\ m_{yy}^{(i)} \\ m_{xy}^{(i)} \end{bmatrix} = D\chi^{(i)} \tag{25}$$

The matrix D in Equation 25 represents the constitutive relationship for the element material. For a plate with constant material properties through the thickness "h," this relationship may be expressed

$$D = \frac{h^3}{12} \begin{bmatrix} C_{11} & C_{12} & C_{13} \\ & C_{22} & C_{23} \\ (\text{Symm.}) & & C_{33} \end{bmatrix} \tag{26}$$

where the coefficients C_{ij} represent the elastic properties. Substituting Equations 20, 22 and 25 into Equation 24 leads to

$$U^{(i)} = \frac{1}{2} r^T T_n^{(i)^T} \int_A \bar{\phi}_x^T D \bar{\phi}_x \, dA \, T_n^{(i)} r$$

or

$$U^{(i)} = \frac{1}{2} r^T K^{(i)} r \tag{27}$$

where

$$K^{(i)} = T_n^{(i)^T} G^{(i)} T_n^{(i)} \tag{28}$$

is the stiffness matrix contribution of Subelement "i" expressed in terms of the nodal Displacements $\mathbf{r}$, and

$$\mathbf{G}^{(i)} = \int_A \bar{\boldsymbol{\phi}}_x^T \mathbf{D}^{(i)} \bar{\boldsymbol{\phi}}_x \, dA \equiv \begin{bmatrix} G_{11}^{(i)} & G_{12}^{(i)} & G_{13}^{(i)} \\ & G_{22}^{(i)} & G_{23}^{(i)} \\ (\text{Symm.}) & & G_{33}^{(i)} \end{bmatrix} \tag{29}$$

If the material properties and thickness are uniform over the area of the subelement, the individual terms of the Matrix $\mathbf{G}^{(i)}$ become

$$G_{ij}^{(i)} = \frac{h^3}{12} C_{ij} \, \mathbf{R}^{(i)}$$

where $\mathbf{R}^{(i)}$ is given by

$$\mathbf{R}^{(i)} = \int_A \bar{\boldsymbol{\phi}}_x^T \bar{\boldsymbol{\phi}}_x \, dA = \frac{A^{(i)}}{12} \begin{bmatrix} 2 & 1 & 1 \\ 1 & 2 & 1 \\ 1 & 1 & 2 \end{bmatrix} \tag{30}$$

If material properties or thickness of the element vary over its area, it is recommended to evaluate the intergral of Equation 29 numerically.

It will be noted that the stiffness matrix of the complete triangle is obtained by merely adding the contributions of the three subelements because they are all expressed in terms of the same set of nodal coordinates. Thus

$$\mathbf{K} = \mathbf{K}^{(1)} + \mathbf{K}^{(2)} + \mathbf{K}^{(3)} \tag{31}$$

ELEMENT STIFFNESS INCLUDING SHEAR DISTORTION

Assumed Displacements

The basic assumption of the element stiffness analysis presented in the preceding paragraphs is the Kirchhoff hypothesis, which may be expressed mathematically as follows:

$$\left.\begin{aligned} w(x,y,z) &= w(x,y) \\ u &= -z \frac{\partial w}{\partial x} = z\,\theta_y \\ v &= -z \frac{\partial w}{\partial y} = -z\,\theta_x \end{aligned}\right\} \tag{32}$$

This assumption imposes the condition that normals to the undeformed plate mid-surface remain undistorted and normal to the deformed mid-surface. The fact that they remain normal during deformation effectively eliminates shear distortion from the assumed behavior, and thus leads to results which are applicable only to relatively thin plates. The theory can be extended to account for shear distortion in an approximate way, however, by adding a simple shear distortion mechanism to the Kirchhoff deformation hypothesis.

The shear distortion mechanism assumed in this study can be explained conveniently by reference to Figure 4a, which represents a cross-section view of a plate element. The rotation of the cross-section is shown to depend on the rotation of the mid-surface $\frac{\partial w}{\partial y}$ plus an additional shear distortion β_y which is assumed to be a simple straight line rotation (uniform shear strain through the thickness). The total rotation ϕ_x thus is given by

$$\phi_x = \frac{\partial w}{\partial y} + \beta_y = \theta_x + \beta_y \tag{33}$$

A similar assumption is made along the other axis, thus

$$\phi_y = -\frac{\partial w}{\partial x} - \beta_x = \theta_y - \beta_x \tag{34}$$

To define this distribution of cross-section rotations through the element field, it is now assumed that the transverse displacements w(x,y) are given by the compatible interpolation functions defined by Equation 17, for each subelement:

$$w^{(i)} = \hat{\phi}^{(i)}_r \tag{35}$$

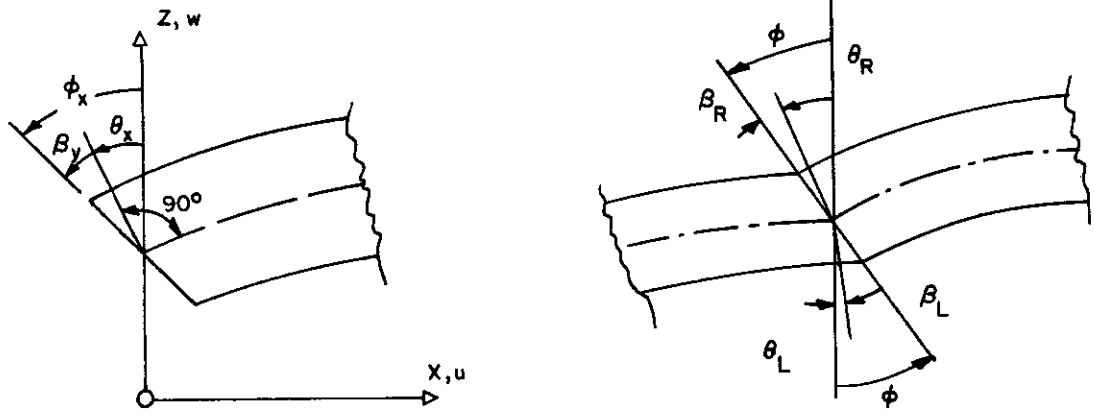

(a) Definition of Mean Shear Distortion (b) Continuity Requirement

Figure 4. Shear Distortion Geometry

In addition, it is assumed that the shear distortions vary linearly over the entire triangle:

$$\begin{bmatrix} \beta_x \\ \beta_y \end{bmatrix} = \begin{bmatrix} \zeta_1 & \zeta_2 & \zeta_3 & 0 & 0 & 0 \\ 0 & 0 & 0 & \zeta_1 & \zeta_2 & \zeta_3 \end{bmatrix} \begin{bmatrix} \beta_{x1} \\ \beta_{x2} \\ \beta_{x3} \\ \beta_{y1} \\ \beta_{y2} \\ \beta_{y3} \end{bmatrix} \tag{36}$$

or symbolically

$$\boldsymbol{\beta} = \boldsymbol{\phi}_\beta \, \mathbf{r}_s \tag{37}$$

Now it is convenient to substitute total rotation of the section ϕ for the slope θ in the nodal degrees of freedom of Equation 35. Thus, using relationships derived from Equation 33 and 34, the following expressions may be defined for each corner nodal point:

$$\begin{bmatrix} \theta_{xi} \\ \theta_{yi} \end{bmatrix} = \begin{bmatrix} \phi_{xi} \\ \phi_{yi} \end{bmatrix} + \begin{bmatrix} -\beta_{yi} \\ +\beta_{xi} \end{bmatrix} \tag{38}$$

while for a typical mid-side node, such as node 4:

$$\theta_4 = \phi_4 - (\beta_{x1} + \beta_{x2}) \frac{c_3}{2} - (\beta_{y1} + \beta_{y2}) \frac{s_3}{2} \tag{39}$$

where $c_3 = a_3/L_3$ and $s_3 = -b_3/L_3$. Similar expressions may be obtained for nodes 5 and 6 by cyclic permutation of indices.

Using these expressions, the interpolation functions for displacement in each subelement Equation 35 may be rewritten as follows:

$$w^{(i)} = \left[\hat{\boldsymbol{\phi}}^{(i)} \,\vdots\, \hat{\boldsymbol{\phi}}_s^{(i)} \right] \left[\frac{\mathbf{r}_B}{\mathbf{r}_s} \right] \tag{40}$$

where

$$\mathbf{r}_B^T = \left[w_1 \; \phi_{x1} \phi_{y1} \; w_2 \phi_{x2} \phi_{y2} \; w_3 \phi_{x3} \phi_{y3} \phi_4 \; \phi_5 \phi_6 \right]$$

$\mathbf{r}_s$ = displacement vector in Eq. 36

$\hat{\boldsymbol{\phi}}^{(i)}$ = interpolation functions of Eq. 17

and

$$\hat{\phi}_s^{(i)T} = \begin{bmatrix} -\phi_{\theta y_1} & -(\phi_{\theta_4} C_3 + \phi_{\theta_6} C_2)/2 \\ -\phi_{\theta y_2} & -(\phi_{\theta_5} C_1 + \phi_{\theta_4} C_3)/2 \\ -\phi_{\theta y_3} & -(\phi_{\theta_6} C_2 + \phi_{\theta_5} C_1)/2 \\ -\phi_{\theta x_1} & -(\phi_{\theta_4} S_3 + \phi_{\theta_6} S_2)/2 \\ -\phi_{\theta x_2} & -(\phi_{\theta_5} S_1 + \phi_{\theta_4} S_3)/2 \\ -\phi_{\theta x_3} & -(\phi_{\theta_6} S_2 + \phi_{\theta_5} S_1)/2 \end{bmatrix} \tag{41}$$

in which the subscripts of the interpolation functions ϕ identify their nodal displacement components. Equations 36, 37 and 40 define completely the deformation of the element, expressing the transverse displacements Equation 40 in terms of 18 nodal displacements, and the shearing distortions Equation 36 in terms only of the 6 nodal shear distortions.

Internal Curvature Field

Where shearing distortions are included in the displacement field, the total curvatures χ^* which define the normal strain distribution depend on both the transverse displacements and the shear distortions as follows:

$$\chi^* = \begin{bmatrix} \frac{\partial \phi_y}{\partial x} \\ \frac{\partial \phi_x}{\partial y} \\ \frac{\partial \phi_y}{\partial y} + \frac{\partial \phi_x}{\partial x} \end{bmatrix} = \begin{bmatrix} \frac{\partial^2 w}{\partial x^2} \\ \frac{\partial^2 w}{\partial y^2} \\ 2\frac{\partial^2 w}{\partial x \partial y} \end{bmatrix} + \begin{bmatrix} \frac{\partial \beta_x}{\partial x} \\ \frac{\partial \beta_y}{\partial y} \\ \frac{\partial \beta_x}{\partial y} + \frac{\partial \beta_y}{\partial x} \end{bmatrix} = \chi + \chi_\beta \tag{42}$$

The first curvature term must be defined separately for each subelement, and from Equation 40 is given by:

$$\chi^{(i)} = \left[T^{(i)} \,\vdots\, T_s'^{(i)} \right] \left[\begin{array}{c} r_B \\ \hline r_s \end{array} \right] \tag{43}$$

where $T^{(i)}$ is given by Equation 18 and $T_s'^{(i)}$ has an equivalent definition in terms of $\hat{\phi}_s^{(i)}$. However, the second curvature term in Equation 42 may be expressed for the entire element, i.e.:

$$\chi_\beta = T_s'' \, r_s \tag{44}$$

where

$$T_s'' = \frac{1}{2A} \begin{bmatrix} b_1 & b_2 & b_3 & 0 & 0 & 0 \\ 0 & 0 & 0 & a_1 & a_2 & a_3 \\ a_1 & a_2 & a_3 & b_1 & b_2 & b_3 \end{bmatrix} \tag{45}$$

applying the derivative definitions of Equation 6 to Equation 36. Thus substituting Equations 43 and 44 into Equation 42 leads to

$$\chi^{*(i)} = \left[T^{(i)} \vdots T_s^{(i)} \right] \begin{bmatrix} r_B \\ \hline r_s \end{bmatrix} \tag{46}$$

where

$$T_s^{(i)} = T_s'^{(i)} + T_s'' \tag{47}$$

Now because these combined curvatures still vary linearly within the subelements, their distribution can be expressed in terms of nodal curvature values as before; i.e. by analogy with Equations 20 and 22:

$$\chi_n''^{(i)} \quad \left[T_n^{(i)} \vdots T_{sn}^{(i)} \right] \begin{bmatrix} r_B \\ \hline r_s \end{bmatrix} \tag{48}$$

and

$$\chi^{*(i)} = \bar{\phi}_x \, \chi_n^{*(i)} \tag{49}$$

Element Stiffness

The strain energy due to bending deformations may be expressed in terms of the bending stiffness matrix by analogy with Equation 31:

$$K_B^{(i)} = \begin{bmatrix} T_n^{(i)T} \\ \hline T_{sn}^{(i)T} \end{bmatrix} \left[G^{(i)} \right] \left[T_n^{(i)} \vdots T_{sn}^{(i)} \right] \equiv \begin{bmatrix} K_{BB} & K_{BS} \\ \hline K_{SB} & K_{SS}' \end{bmatrix} \tag{50}$$

in which $\mathbf{G}^{(i)}$ is exactly as in Equation 30. An additional strain energy contribution U_s results from the shear distortion, however, which is given as follows:

$$U_s = \frac{1}{2} \int_A \mathbf{Q}^T \boldsymbol{\beta} \, dA \tag{51}$$

in which the shearing forces $\mathbf{Q}$ are

$$\mathbf{Q} \equiv \begin{bmatrix} Q_x \\ Q_y \end{bmatrix} = \mathbf{D}_s \boldsymbol{\beta} \tag{52}$$

In this expression, $\mathbf{D}_s$ represents the shear distortion constitutive relationship. For a plate with uniform properties through the thickness, and assuming that z is a principal elastic direction, it may be expressed:

$$\mathbf{D}_s = h \begin{bmatrix} C_{44} & C_{45} \\ C_{45} & C_{55} \end{bmatrix} \tag{53}$$

in which C_{ij} are material constants.

Introducing Equations 53, 52 and 37 into Equation 51 leads to

$$U_s = \frac{1}{2} \mathbf{r}_s^T \int_A \boldsymbol{\phi}_\beta^T \mathbf{D}_s \boldsymbol{\phi}_\beta \, dA \, \mathbf{r}_s$$

or

$$U_s = \frac{1}{2} \mathbf{r}_s^T \mathbf{K}''_{ss} \mathbf{r}_s \tag{54}$$

where $\underline{K''_{ss}}$ is the shear stiffness matrix. In the case where material properties and thickness are uniform over the element, the shear stiffness becomes

$$\mathbf{K}''_{ss} = h \begin{bmatrix} C_{44}\mathbf{R} & C_{45}\mathbf{R} \\ C_{45}\mathbf{R} & C_{55}\mathbf{R} \end{bmatrix} \tag{55}$$

in which $\mathbf{R}$ is given by Equation 30. For nonuniform thickness or material properties, the integral should be evaluated numerically.

The total stiffness is obtained finally by superposition of the bending and shear contributions,

$$\mathbf{K} = \left[\begin{array}{c|c} \mathbf{K}_{BB} & \mathbf{K}_{BS} \\ \hline \mathbf{K}_{SB} & (\mathbf{K}'_{SS} + \mathbf{K}''_{SS}) \end{array}\right] \tag{56}$$

in which it should be noted that the bending terms must be computed separately for each subelement and added, whereas the shear stiffness term K''_{SS} may be computed for the entire element.

Condensation of Shear Distortion Degrees of Freedom

The element stiffness matrix of Equation 56 represents the element force-displacement relationship, which may be expressed as follows:

$$\begin{bmatrix} P_B \\ P_S \end{bmatrix} = \begin{bmatrix} K_{BB} & K_{BS} \\ K_{SB} & K_{SS} \end{bmatrix} \begin{bmatrix} r_S \\ r_S \end{bmatrix} \tag{57}$$

in which $K_{SS} = K'_{SS} + K''_{SS}$. A total of 18 degrees of freedom are included in this relationship, 6 shear distortion components r_S in addition to the 12 basic translation and rotation displacements of the nodes. At this point, however, it should be noted that the shear distortion angle β need not be continuous between adjacent elements. As shown in Figure 4b, the total rotation ϕ must be the same for two adjacent elements in order to satisfy compatibility conditions, but β and θ need not be the same. Consequently, the shear distortion degrees of freedom are not needed to achieve compatibility and they may be eliminated from the element by static condensation.

As a result of the condensation process, the modified element stiffness relationship becomes:

$$\overline{P} = \overline{K}\, r \tag{58}$$

in which

$$\begin{aligned} \overline{K} &= K_{BB} - K_{BS}\, K_{SS}^{-1}\, K_{SB} \\ \overline{P} &= P_B - K_{BS}\, K_{SS}^{-1}\, P_S \end{aligned} \tag{59}$$

It is of interest to note that the degrees of freedom of this reduced element stiffness matrix are exactly equivalent to those of the original LCCT-12 element; thus, an element including this shear distortion capability can easily be incorporated into existing plate bending analysis programs based on the original element.

GENERAL QUADRILATERAL ELEMENT Q-19

Although the LCCT-12 element employs an optimum compatible cubic displacement field and, therefore, will yield the best possible results for a given triangular element mesh involving compatible cubic displacements, its mid-point nodes are a somewhat undesirable feature. They tend to complicate mesh generation procedures, increase the band width of the assembled equation systems, and require special identification in the development of computer programs. To overcome these disadvantages, while retaining most of the flexibility of the LCCT-12 element, it is convenient to develop a special version of the element by constraining the normal slope to vary linearly along one side.

Consider, for example, Subelement 3 of the element shown in Figure 3a. The mid-side node 4 of this subelement can be eliminated by introducing the condition that its value is the average of the corresponding slopes at nodes 1 and 2,

$$\theta_4 = \theta_{x4}\, c_3 - \theta_{y4}\, s_3 = (\theta_{x1}+\theta_{x2})\frac{c_3}{2} - (\theta_{y1}+\theta_{y2})\frac{s_3}{2} \qquad (60)$$

where c_3 and s_3 are the same as in Equation 39. Using this condition, the displacement interpolation expressions in Equation 17 can be reduced to only 11 components, and the stiffness matrix thus reduced accordingly.

The resulting partially constrained element is designated LCCT-11. (Similar constraints must be applied to the other sides to develop the LCCT-10 and LCCT-9 elements.) Four LCCT-11 elements may then be assembled into the Q-19 quandrilateral having no mid-side nodes on the exterior edges as shown in Figure 5. Although this element has 19 degrees of freedom, the 7 internal degrees of freedom of the assemblage are eliminated by a static condensation process equivalent to Equation 56 before the quadrilateral is assembled into the complete structure. Thus, the final quadrilateral has only 12 degrees of freedom, corresponding to a translation and two rotations at each node. It is a fully compatible element, having linear variations of normal slopes along all exterior edges.

Also it should be noted that triangular elements including shear distortion effects can be assembled to form a quadrilateral element in a similar fashion. In this case, however, it has been found most convenient to condense the shear distortion degrees of freedom at the quadrilateral assemblage level rather than in the individual triangles.

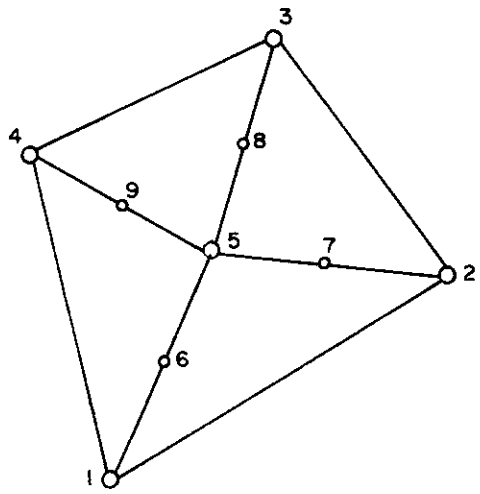

Figure 5. Quadrilateral Q-19 Assembled with 4 LCCT-11 Elements

SECTION III

RESULTS OF ANALYSES WITH THE Q-19 ELEMENT

STATIC PLATE BENDING

Neglecting Shear

In order to evaluate the accuracy obtainable with the Q-19 quadrilateral element, a series of convergence studies were made of the central deflection developed in a square plate. Both uniform pressure and concentrated central loading cases were considered; boundary conditions were both simply supported and clamped. Because of double symmetry, only one-quarter of the plate was considered in the analyses.

The computed central deflections are presented in Figure 6, the abscissa in the graphs representing the number of elements along one side of the square mesh. Results for the

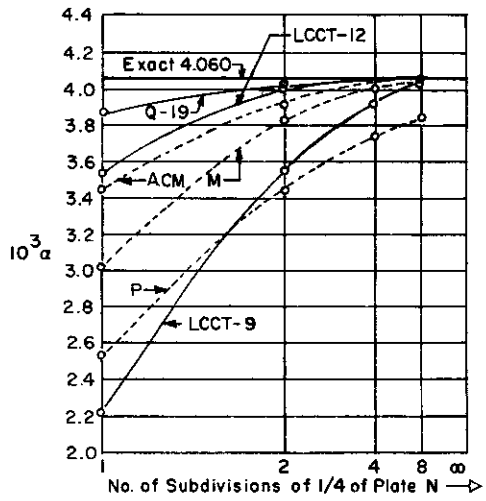

(a) Central Deflection $w = \alpha\, q\, a^4/D$ of Simply Supported Square Plate Under Uniform Load q

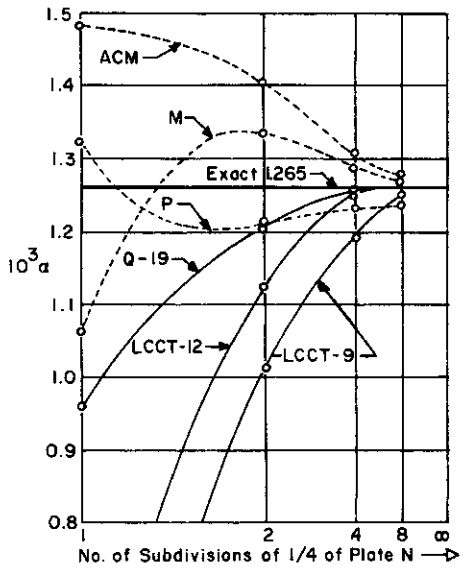

(b) Central Deflection $w = \alpha\, q\, a^4/D$ of Square Clamped Plate Under Uniform Load q

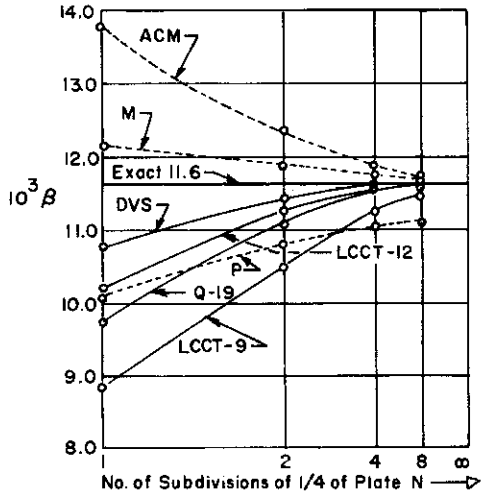

(c) Central Deflection $w = \beta\, P\, a^2/D$ of Simply Supported Square Plate Under Concentrated Central Load P

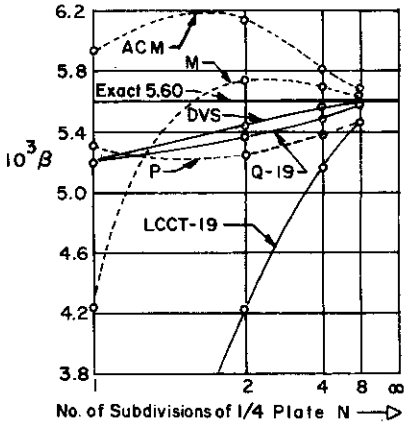

(d) Central Deflection $w = \beta\, P\, a^2/D$ of Clamped Square Plate Under Concentrated Central Load P

MEANING OF SYMBOLS	
M, ACM	Incompatible but complete rectangular elements (see Ref. 12); 12 external D. F.
P	Compatible but incomplete rectangular element (see Ref. 12); 12 external D. F.
LCCT-9	Two LCCT-9 triangles (labeled HCT in Ref. 12); 12 external D. F.
LCCT-12	Two LCCT-12 triangles; 16 external and 1 internal D. F.
Q-19	Four LCCT-11 triangles; 12 external and 7 internal D. F.
DVS	Compatible quadrilateral from Refs 14 and 23; 16 external D. F.
-----	Indicates a rectangular element constructed with a single C^2 expansion.
———	Denotes a triangular or quadrilateral element constructed with a C^1 expansion.

Figure 6. Convergence Study of Various Plate Bending Elements

elements described in this paper are labeled Q-19, LCCT-12, and LCCT-9. Also shown are results for rectangular elements presented in Reference 12 (note that LCCT-9 was labeled HCT there), as well as a new quadrilateral DVS from Reference 23. The superiority of Q-19 over any other quadrilateral element with 12 degrees of freedom is clearly evident — the improvement over LCCT-9 is quite marked. It may be noted that DVS gives slightly better results than Q-19, but it has 16 degrees of freedom, including mid-side nodes which greatly hamper its computational efficiency.

A second static analysis example is presented in Figure 7, the rectangular plate being loaded uniformly, simply supported at two sides, clamped and free at the other two edges (problem taken from Reference 25). Results of a 4 x 4 mesh of LCCT-12 elements (2 triangles to each square) are shown. Displacements are essentially exact, while the moments are very close to the exact results. Computed moments from an 8 x 8 mesh are indistinguishable from the exact curves except at the edges. It is probable that the Q-19 element would have given still better results and would have required less computer effort. (However, the 8 x 8 LCCT-12 analysis required only 48 seconds on an IBM 7094 computer.)

Including Shear Distortion

Results of the first test of the shear distortion capability of the Q-19 element are presented in Figure 8. The structure is a circular plate, simply supported at the outer boundary with a transverse shearing force applied uniformly about the edge of a central hole (Reference 25). Taking advantage of rotational symmetry about the hole, it was necessary to consider only a sector of the plate in the finite element idealization, as shown. Comparison of the finite element results with the exact theory demonstrates the effectiveness of the assumed shear distortion mechanism.

The shear stress resultants Q_x computed in a second analysis with the Q-19 shear distortion element are shown in Figure 9. The structure in this case was a square, simply supported plate subjected to a uniform loading (Figure 9a) and a central concentrated loading (Figure 9b). The mesh was 8 x 8 on the 1/4 plate system; the plate thickness was 1/10 of the total span. Although no other solution is available to compare with these results, it is of interest to note that shear distortion caused an increase in central deflection over the results of Figure 6 of 10% under uniform loading and 294% with the concentrated load.

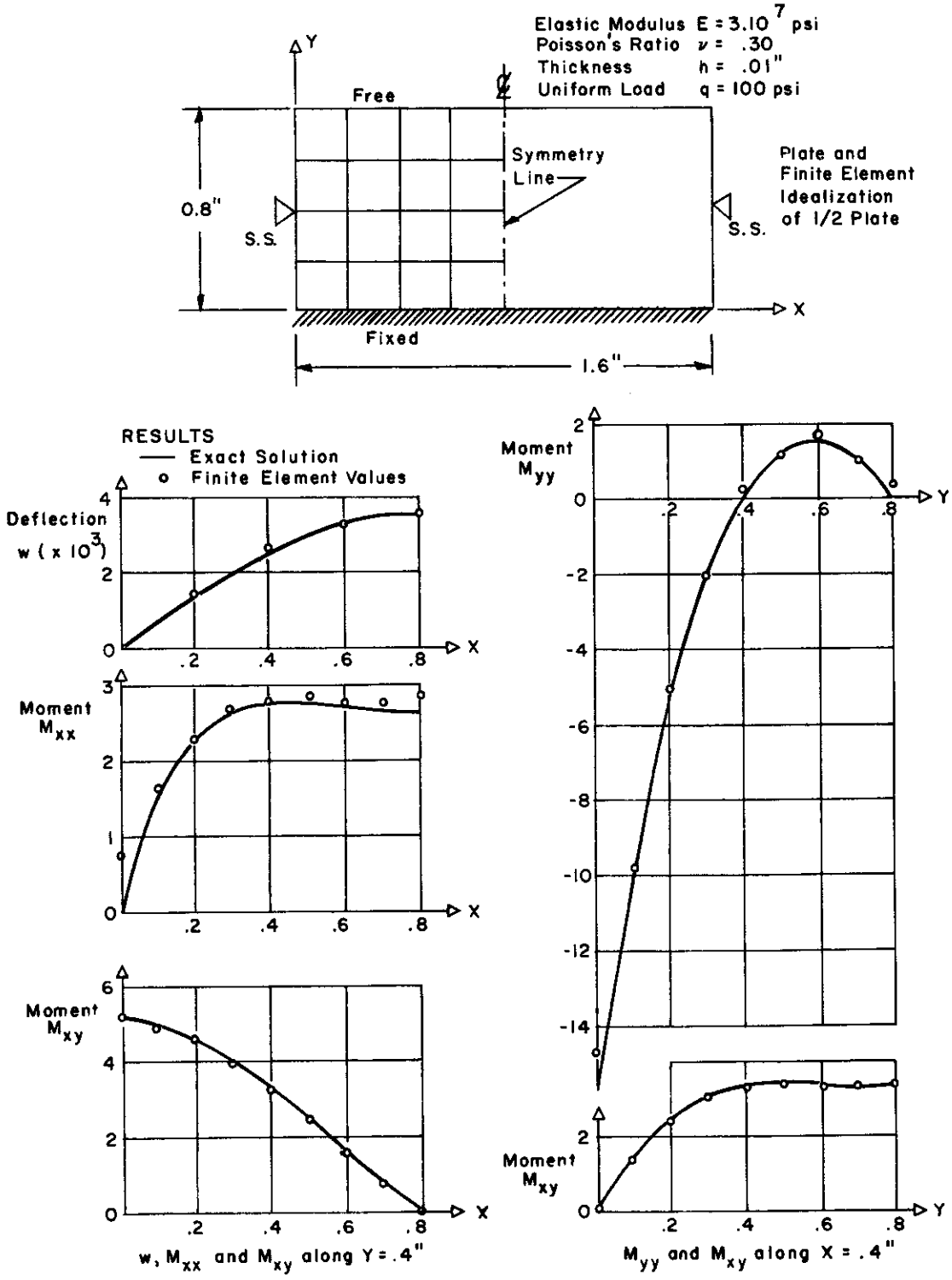

Figure 7. Analysis of a S.S-Clamped-Free Rectangular Plate

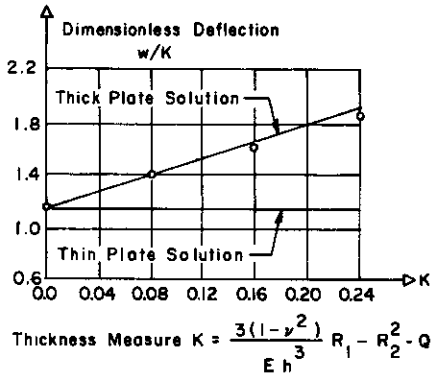

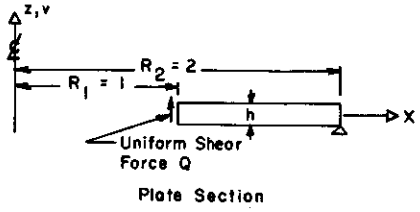

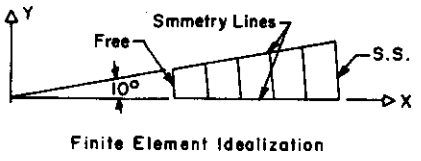

Figure 8. Analysis of Thick Annular Plate

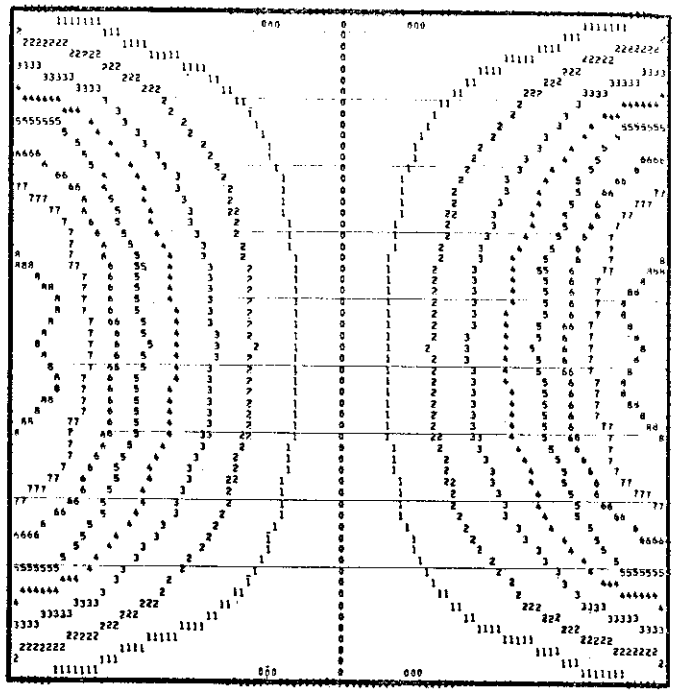

(a) Uniform Load

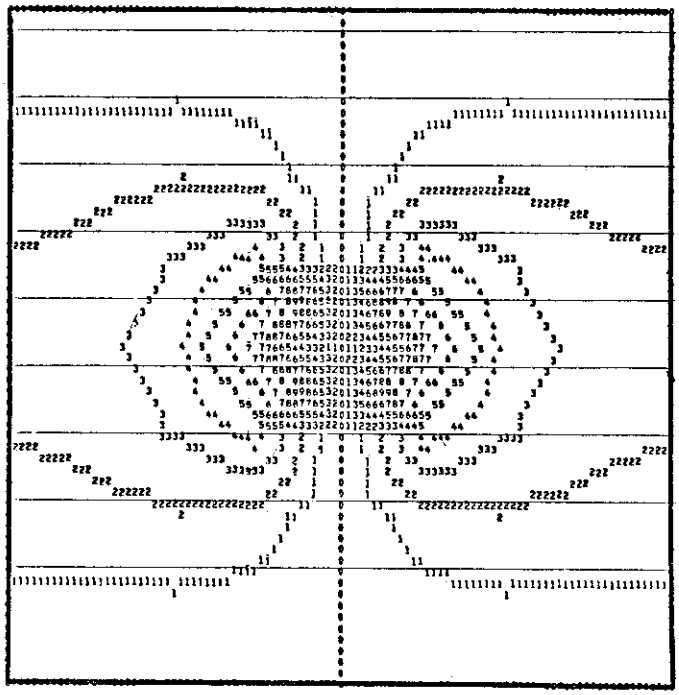

(b) Concentrated Central Force

Figure 9. Computer Plots of the Transverse Shear Q-X in a Simply Supported Square Plate

ANALYSIS OF PLATE VIBRATIONS

Eigenvalue Equation

The equation of motion of a discrete coordinate system in free vibration may be written:

$$\mathbf{K}\,\mathbf{v} = \omega^2\,\mathbf{M}\,\mathbf{v} \tag{61}$$

in which $\mathbf{K}$ represents the stiffness of the assembled structure, $\mathbf{M}$ is the inertia matrix of the system, ω is the circular frequency of vibration and $\mathbf{v}$ is the vibration mode shape. The stiffness matrix used here is the same as would be used for a static analysis; in a finite element solution it is formed by appropriate superposition of the individual element stiffnesses. The mass matrix may similarly be formed by assembly of the individual element mass matrices. The first problem to be considered, then, is the definition of the element mass matrix.

Element Mass Matrix

Two different formulations of the element mass have been used extensively in finite element studies: the lumped mass (LM) and the consistent mass (CM) idealizations. For the lumped mass approach, it is assumed that the mass is concentrated in points at the nodes of the element, with nodal values chosen to be statically equivalent to the actual mass distribution. In the case of a uniform triangular element, one third of the mass is concentrated at each corner. The LM matrix is diagonal in form, with non-zero terms associated only with the translational degrees of freedom.

The CM matrix may be derived from the displacement interpolation functions assumed for the element. Using the displacements given in Equation 17, the consistent mass matrix for each subelement is

$$\mathbf{M}^{(i)} = \int_A \rho\, \hat{\boldsymbol{\phi}}^{(i)T}\, \hat{\boldsymbol{\phi}}^{(i)}\, dA \tag{62}$$

where ρ is the mass per unit area. The complete element CM matrix is obtained by adding the contributions of the individual subelements (by analogy with Equation 32). The CM matrix is fully populated, in contrast to the diagonal LM matrix.

In forming the LM matrix for the Q-19 element, it was considered desirable to retain the mass at the interior nodal point; thus, this nodal point was retained also in the stiffness

Quadrilateral Idealizations:

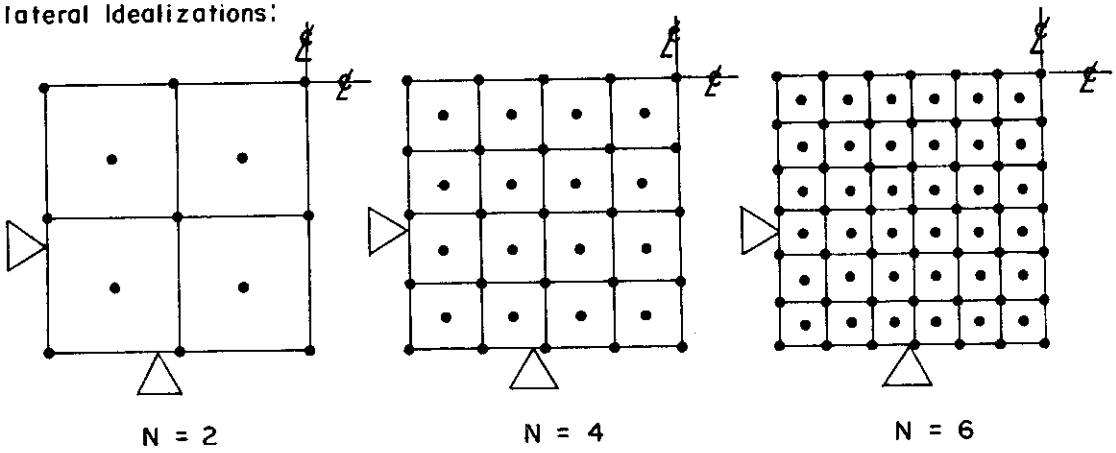

Degrees of Freedom for 1/4 Plate:

Analysis	Mode Type	N = 2	N = 4	N = 6
Liquid Mass	S-S A-S	13 8	41 32	83 72
Cons. Mass	S-S A-S	24 22	96 92	216 210

Red. Freq.	Mode Type	Theory m^2+n^2	N = 2		N = 4		N = 6	
			LM	CM	LM	CM	LM	CM
λ_{11}	S - S	2.000	2.034	2.031	2.007	2.007	2.001	2.001
λ_{12}	A - S	5.000	5.142	5.135	5.032	5.031	5.013	5.012
λ_{13}	S - S	10.000	10.185	10.390	10.076	10.078	10.032	10.032
λ_{23}	A - S	13.000	13.499	14.028	13.317	13.289	13.131	13.125
λ_{14}	A - S	17.000	—	19.014	17.136	17.176	17.059	17.065
λ_{33}	S - S	18.000	17.117	19.747	18.733	18.647	18.305	18.283
λ_{34}	A - S	25.000	23.672	29.880	26.283	26.153	25.557	25.509
λ_{15}	S - S	26.000	30.267	28.954	26.186	26.390	26.095	26.127

Figure 10. Reduced Frequencies $\lambda_{mn} = \omega_{mn} a^2 \sqrt{\frac{\rho h}{D}}$ of S.S. Square Plate

Quadrilateral Idealizations:

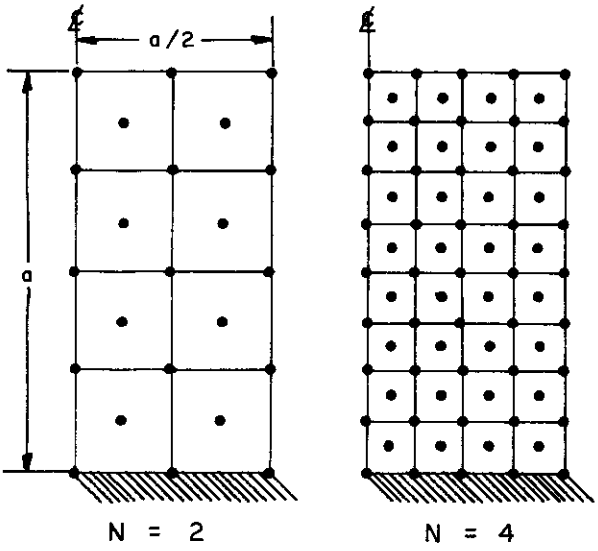

Degrees of Freedom for 1/2 Plate:

Analysis	Mode	N = 2	N = 4
LN	S	20	72
	A	16	64
CM	S	56	208
	A	52	200

Poisson's ration $\nu = 0.29$

Rod. Freq.	Mode Type	Tests		Theory		N = 2		N = 4	
		Daily (1)	Gustafson (2)	Barton (3)	Plass (4)	LM	CM	LM	CM
λ_1	S	3.37	3.35	3.494	3.44	3.430	3.477	3.441	3.453
λ_2	A	8.26	8.53	8.547	8.27	8.388	8.693	8.501	8.577
λ_3	S	20.55	20.90	21.44	20.14	20.168	21.453	21.029	21.362
λ_4	S	27.15	26.72	27.46	—	25.254	27.629	26.729	27.334
λ_5	A	29.75	30.61	31.17	—	29.493	31.854	30.718	31.274

(1) Report DRL-231, Def. Res. Lab., University of Texas, Austin, 1949
(2) J. Aero. Sci., 20, 331, 1951
(3) J. Appl. Mech., 18, 2, 1951
(4) J. ASME, March 1962, p. 315.

Figure 11. Reduced Frequencies $\lambda_n = \omega_n a^2 \sqrt{\frac{\rho h}{D}}$ of Square Cantilever Plate

Quadrilateral Idealizations:

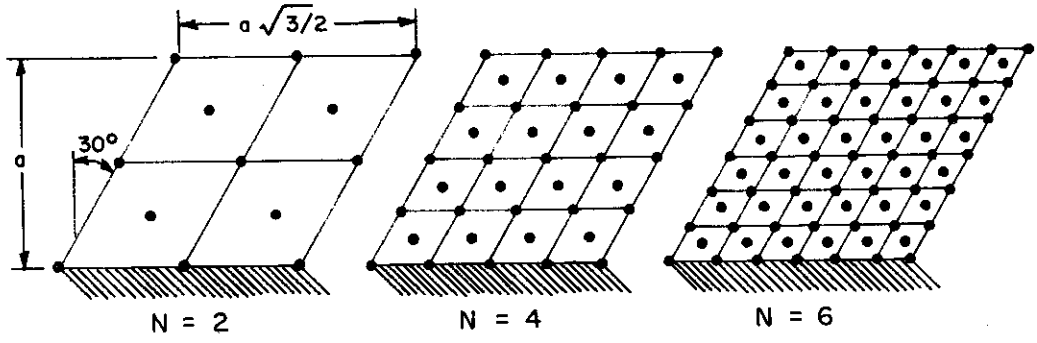

Degrees of Freedom for IM Analysis

10 41 85

Poisson's ratio $\nu = 0.29$

Red. Freq.	Tests Dally & Ripperger (1)	Theory Barton (2) (Rayleigh – Ritz)	Lumped Mass Analysis		
			N = 2	N = 4	N = 6
λ_1	3.82	3.96	3.897	3.928	3.928
λ_2	9.23	10.19	8.606	9.303	9.409
λ_3	24.51	—	22.041	24.231	24.987
λ_4	25.51	—	20.487	25.051	25.558
λ_5	40.64	—	31.157	39.501	40.666

(1) Report DRL – 231, Def. Res. Lab., University of Texas, Austin, 1949
(2) J. Appl. Mech., 18, 2, 1951

Figure 12. Reduced Frequencies $\lambda_n = \omega_n a^2 \sqrt{\frac{\rho h}{D}}$ of a Rhombic Cantilever Plate (Skewangle = 30°)

Quadrilateral Idealizations:

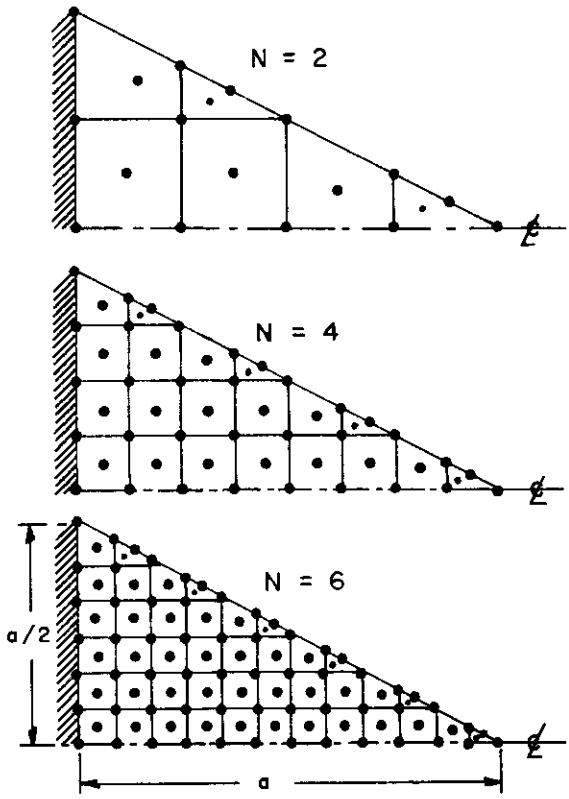

Degrees of Freedom for 1/2 Plate:

Analysis	Mode	N=2	N=4	N=6
LM	S	16	48	96
	A	12	40	84
CM	S	44	136	276
	A	40	128	264

Poisson's ratio $\nu = 0.29$

Red. Freq.	Mode Type	Tests Gustafson (1)	Theory Andersen (2)	N = 2		N = 4		N = 6	
				LM	CM	LM	CM	LM	CM
λ_1	S	6.61	7.149	6.632	6.859	6.697	6.739	6.613	6.631
λ_2	A	28.50	30.803	27.330	29.583	28.534	29.305	28.904	29.225
λ_3	S	29.00	61.131?	27.687	30.160	28.848	29.535	29.022	29.392
λ_4	S	69.30	—	63.759	72.114	68.552	70.495	69.313	70.179
λ_5	A	75.50	—	74.866	80.835	74.465	78.305	75.510	77.751

(1) J. Aero. Sci., 20, 331, 1951
(2) J. Appl. Mech., 21, 4, 1954

Figure 13. Reduced Frequencies $\lambda_n = \omega_n a^2 \sqrt{\frac{\rho h}{D}}$ of Isosceles Cantilever Plate

matrix for vibration analysis. The CM matrix for the Q-19 element was developed by assembling the CM matrices for 4 LCCT-9 elements; i.e. the interior mid-side nodes were omitted. The stiffness matrix used in the CM vibration studies was the same as that used in the LM studies, the assembled CM matrix for the complete structure had a similar banded form to that of the stiffness matrix.

Analytical Results

The vibration frequencies computed for a series of plate systems are presented in Figures 10-13. The systems comsidered were a rectangular simply supported plate, a rectangular cantilever, a skewed cantilever, and a triangular cantilever. Different mesh sizes were used in each case to demonstrate convergence, and both LM and CM idealizations were utilized. Also shown are results of other analyses and some experimental results. It is apparent in these figures that the results of the finite element analysis are excellent, giving reliable agreement with experiments and with exact theories. Of greatest significance is the comparison between LM and CM analyses; in almost every case, the LM result for a given mesh size is more accurate than the CM value, in spite of the fact that the CM systems involved 2 to 3 times more degrees of freedom. The only advantage of the CM result is that it provides an upper bound to the exact value, while the LM result may be either low or high. Plots of a few mode shapes for the skewed cantilever plate are shown in Figure 14.

ANALYSIS OF PLATE BUCKLING

Eigenvalue Equation

The linearized buckling analysis of plates leads to an eigenvalue equation which is very similar in form to the vibration equation; it may be written:

$$\mathbf{K}\,\mathbf{v} = \lambda\,\mathbf{K}_G\,\mathbf{v} \tag{63}$$

in which $\mathbf{K}_G$ is the initial stress (or geometric stiffness) matrix of the system and λ is the critical load factor, with other terms as in Equation 59. Since the elastic stiffness matrix $\mathbf{K}$ used here is the same as that used for ordinary static analyses, the essential problem in the stability analysis is evaluation of the initial stress matrix.

Initial Stress Matrix

The initial stress matrix for plate buckling analysis may be interpreted physically as the out-of-plane nodal forces resulting from the action of existing in-plane (membrane) stresses

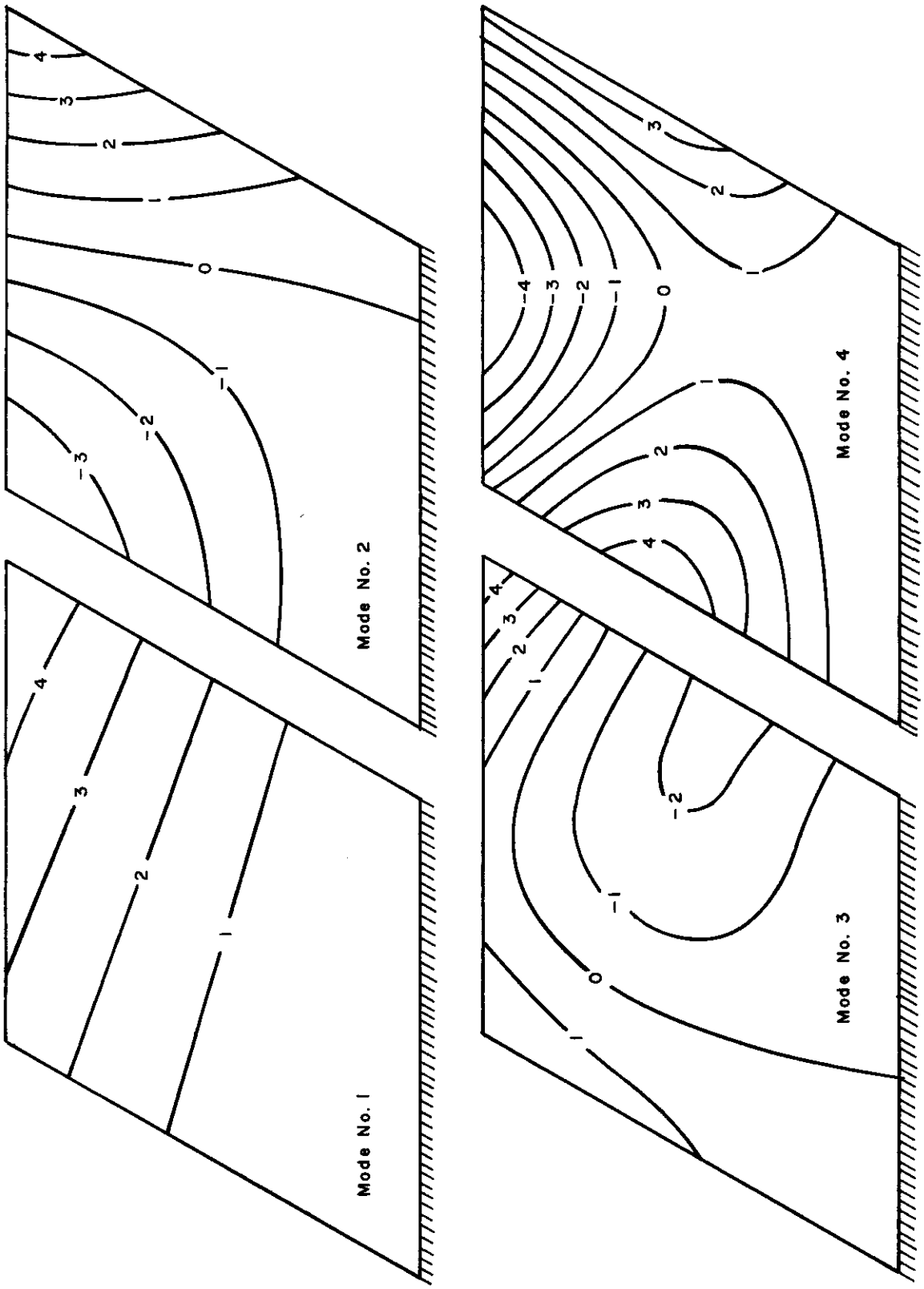

Figure 14. Vibration Modes of Rhombic Cantilever Plate

on the out-of-plane displacements. It may be calculated, in general, from an expression of the form

$$K_G = \int_A \begin{bmatrix} \phi_{w,x}^T & \phi_{w,y}^T \end{bmatrix} \begin{bmatrix} N_x & N_{xy} \\ N_{xy} & N_y \end{bmatrix} \begin{bmatrix} \phi_{w,x} \\ \phi_{w,y} \end{bmatrix} dA \tag{64}$$

in which N_x, N_{xy} and N_y represent the membrane stress resultant components existing in the element, and $\phi_{w,x}$ and $\phi_{w,y}$ represent the slopes of the assumed displacement interpolation functions ϕ_w in the x and y directions.

As was the case in the development of mass matrices, different levels of approximation can be employed in the formulation of the initial stress matrices; i.e., different orders of displacement expansions may be used for ϕ_w. The simplest available approximation is based on a single linear expansion (SL) for the entire triangle; i.e., for this case

$$\phi_w \text{ (SL)} = \begin{bmatrix} \zeta_1 & \zeta_2 & \zeta_3 \end{bmatrix} \tag{65}$$

The next higher order of practical usage is the single cubic expansion (SC) where the displacements are those assumed in developing the incompatible triangle (here denoted BCIZ) of Reference 13. The highest order considered here is the compatible cubic expansion, in which the interpolation functions are those defined for each subelement in Equation 17, i.e.,

$$\phi_w^{(i)} \text{ (LCCT)} = \hat{\phi}^{(i)} \tag{66}$$

In the case where the initial stress matrix is based on the same displacement expansions used in deriving the stiffness matrix, it may be termed the consistent initial stress matrix; thus the consistent K_G for use with the LCCT elements is obtained by using Equation 66 in Equation 64, whereas the consistent K_G for an analysis in which the stiffness matrix was based on the single cubic expansion would require the use of that same expansion in Equation 64.

Analytical Results

Results of a series of buckling analyses of three different rectangular plates are presented in Figure 15. Part "a" shows the case of a square simply supported plate subjected to uniaxial membrane stress N_x; Part "b" is a square clamped plate with uniform biaxial membrane stresses $N_x = N_y$; and Part "c" is a simply supported rectangular plate (5/4 aspect ratio) subjected to uniform shear stress N_{xy}. In each case, five different finite element types

CASE	Coeff. k in $\sigma_{cr} = k\frac{\chi^2 D}{a^2 h}$	Mesh over entire plate	FINITE ELEMENT RESULTS									
			QUADRILATERAL Q-19						BCIZ (Ref. 13)		ACM (Ref. 33)	
			Single Linear (SL) Expansion for K_G		Single Cubic (SL) Expansion for K_G		Consistent K_G		Consistent K_G		Consistent K_G	
			K	error	K	error	K	error	K	error	K	error
(a) S.S. Square Plate is Uniaxial Compression 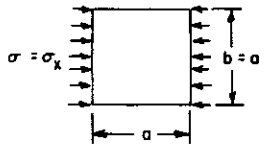	4.000	4 x 4 *	4.356	+8.9%	4.125	+3.2%	4.126	+3.2%	3.883	-2.9%	3.770	-5.8%
		8 x 8	4.083	+2.1%	4.031	+0.8%	4.031	+0.8%	3.883	-2.9%	3.933	-1.7%
		12 x 12	4.038	+0.9%	4.015	+0.4%	4.015	+0.4%	3.884	-2.9%	3.997	-0.6%
		16 x 16	4.021	+0.5%	4.007	+0.2%	4.007	+0.2%	3.884	-2.9%		
		20 x 20	4.013	+0.3%	4.0048	+0.12%	4.0050	+0.12%	3.885	-2.9%		
		28 x 28			4.0025	+0.06%						
(b) Clamped Square Plate in Biaxial Compression 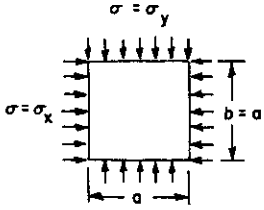	5.310**	4 x 4 *	6.255	+18%	5.625	+5.9%	5.625	+5.9%	5.043	-5.0%	4.975	-6.3%
		8 x 8	5.540	+4.8%	5.399	+1.7%	5.399	+1.7%	5.119	-3.6%	5.160	-2.9%
		12 x 12	5.406	+1.8%	5.345	+0.7%	5.345	+0.7%	5.134	-3.3%		
		16 x 16	5.359	+0.9%	5.325	+0.28%	5.326	+0.28%	5.140	-3.2%		
		20 x 20	5.335	+0.5%	5.318	+0.15%	5.318	+0.15%	5.144	-3.1%		
		28 x 28			5.132	+0.04%						
(c) S.S. Rectangular Plate (b/a = .8) under Pure Shear 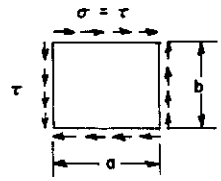	7.78**	2 x 2	30.374		22.247		22.836		10.144			
		4 x 4	10.274	+31	8.756	+10.4%	8.584	+10.5%	7.692	-1.0%	6.945	-10.7%
		6 x 6	8.777	+12.9%	8.107	+3.1%	8.109	+3.1%	7.563	-2.7%	7.247	-5.2%
		8 x 8	8.314	+7.0%	7.952	+2.3%	7.953	+2.3%	7.543	-2.9%	7.450	-4.1%
		10 x 10	8.111	+4.3%	7.884	+1.4%	7.884	+1.4%	7.540	-3.0%		
		14 x 14			7.826	+0.5%						

NOTES: (*) Only 1/4 of the plate was actually considered.

(**) These values (calculated from energy methods) are also approximations, and the last digit is not guaranteed.

Figure 15. Buckling Analysis of Three Model Plate Problems

were employed for each of several different mesh systems. Using the Q-19 stiffness, initial stress stiffnesses were computed for the SL, SC, and the consistent displacement expansions. In addition, the BCIZ and ACM elements were used with their corresponding consistent initial stress matrices (the latter results being from Reference 33).

Comparison of these results shows that the Q-19 element with the SC or consistent initial stress matrices gave consistently superior results. The single linear expansion $\mathbf{K}_G(SL)$, although easily formed, is not sufficiently accurate to be recommended in general. A curious feature of the BCIZ results is that they do not show regular improvement with mesh refinement — in fact, they tend to give poorer results with the finer meshes in the shear stress loading. In these analyses, the ACM results are seen to be well behaved, although not as accurate as the Q-19 results; in addition, it must be remembered that they also impose a significant geometric limitation because of their rectangular shape.

A significant conclusion that may be drawn from these results is that the initial stress matrix based on the single cubic expansion is as effective as the consistent stiffness for the Q-19 element. This initial stress matrix is highly recommended, therefore, because it requires much less computational effort to formulate. From this observation, it appears that lower order expansions may be used generally in deriving the geometric stiffness than are required in the formulation of the elastic stiffness. This conclusion is parallel to the observation made in the vibration analyses regarding the relative merits of the LM and CM matrices, where the lower order approach also was considered superior.

The computed buckled shapes for the fine mesh Q-19 analyses of these three structural systems are shown in Figure 16. Also shown is the buckled shape for a shear loaded rectangle with an aspect ratio of 5/2, showing the two lobe deflection pattern.

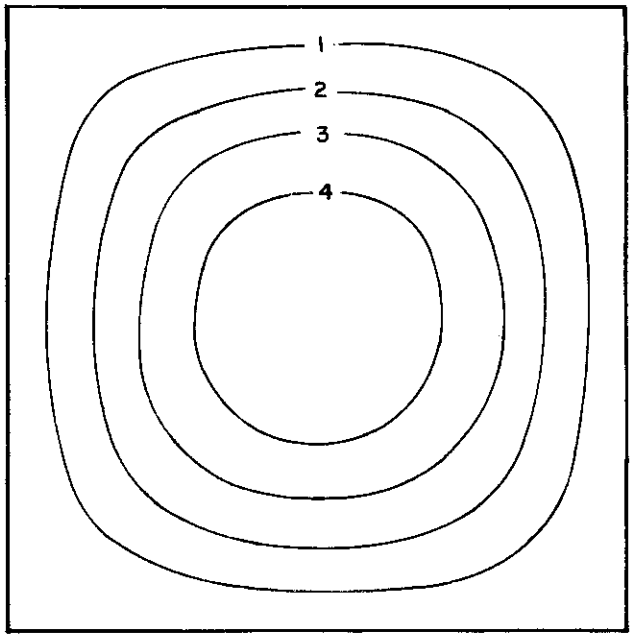

(A) Simply Supported Square Plate Under Uniform Uniaxial Compression Sig - XX

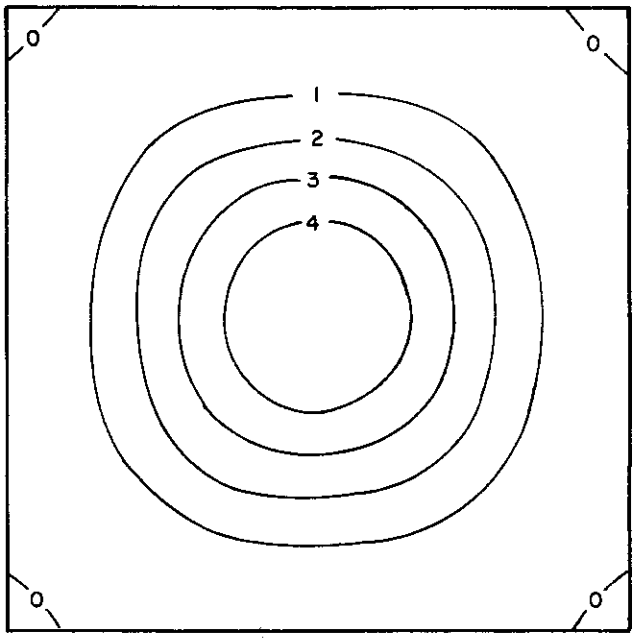

(B) Clamped Square Plate Under Uniform Biaxial Compression

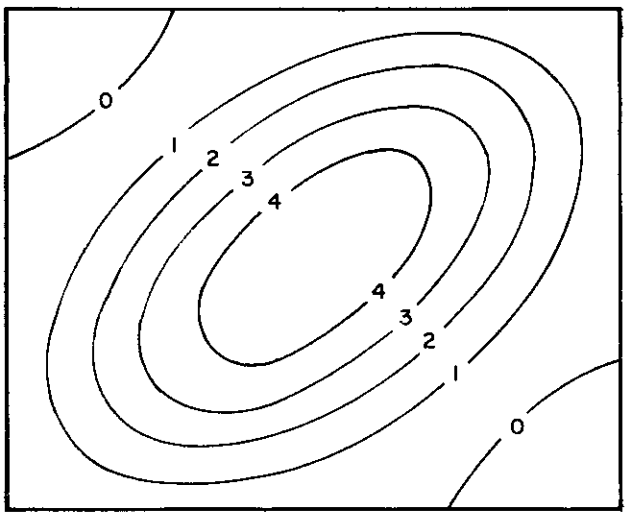

(C) Simply Supported Rectangular Plate (8/A = 0.8) Under Pure Shear

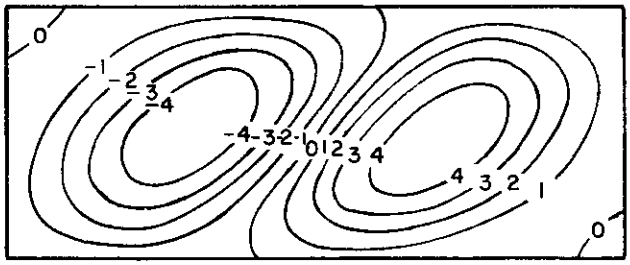

(D) Simply Supported Rectangular Plate (8/A = 0.4) Under Pure Shear

Figure 16. Computer Plots of Plate Buckling Modes

CONCLUSIONS

The principal conclusions which may be drawn from the study reported here are as follows:

(1) The Q-19 fully compatible quadrilateral appears to be the most efficient general plate bending element yet developed. Because it has only 12 degrees of freedom when assembled into the complete system, and no mid-side nodes, it offers maximum computational efficiency.

(2) The shear distortion mechanism incorporated into this element provides a reasonable approximation of thick plate behavior, while leaving the general form of the element stiffness matrix unchanged. Thus, it may easily be incorporated into existing plate analysis programs.

(3) The plate vibration studies reported here demonstrate that a lumped mass matrix is more efficient in representing inertial effects than a consistent mass matrix. (The same relative behavior had been observed previously in dynamic axi-symmetric analyses.)

(4) A similar conclusion can be drawn from the plate buckling results: the initial stress matrix based on a single cubic expansion is computationally more efficient than the higher order consistent matrix for the Q-19 element.

It also is of interest to report that the LCCT and Q-19 elements have been used extensively and effectively in providing the bending stiffness in finite element thin shell analysis programs (Reference 34).

REFERENCES

1. Turner, M. J., Clough, R. W., Martin, H. C. and Topp, L. J., "Stiffness and Deflection Analysis of Complex Structures," J. Aero. Sci., Vol. 23, No. 9, pp. 805-823, 1956.

2. Gallagher, R. H., A Correlation Study of Methods of Matrix Structural Analysis, AGARDograph 69, Pergamon Press, Oxford, 1964.

3. Chapters 5, 6 and 7 of Stress Analysis edited by O. C. Zienkiewicz and G. S. Hollister, John Wiley and Sons, 1965.

4. Zienkiewicz, O. C. and Cheung, Y. K., The Finite Element Method in Structural and Continuum Mechanics, McGraw-Hill Ltd., London, 1967.

5. Melosh, R. J., "Basis for Derivation of Matrices for the Direct Stiffness Method," AIAA Journal, Vol. 1, pp. 1631-1637, 1963.

6. McLay, R. W., An Investigation Into the Theory of the Displacement Method of Analysis for Linear Elasticity, Ph.D. Thesis, University of Wisconsin, Madison, Wis., 1963.

7. de Arantes e Oliveira, E. R., "Mathematical Foundations of the Finite Element Method," Lab. Nacional de Engenharia Civil, Lisbon, 1967.

8. Felippa, C. A. and Clough, R. W., "The Finite Element Method in Solid Mechanics," AMS Symposium on the Numerical Solution of Field Problems in Continuum Mechanics, Durham, N.C., April 1968.

9. Papenfuss, S. W., Lateral Plate Deflection by Stiffness Matrix Methods with Application to a Marquee, M.S. Thesis, Department of Civil Engineering, Univ. of Washington, Seattle, Wash., 1959.

10. Melosh, R. J., "A Stiffness Matrix for the Analysis of Thin Plates in Bending," J. Aero. Sci., 28, 34, 1961.

11. Adini, A. and Clough, R. W., "Analysis of Plate Bending by the Finite Element Method," Report to the Nat. Sci. Foundation, Grant G7337, 1961.

12. Clough, R. W. and Tocher, J. L., "Finite Element Stiffness Matrices for the Analysis of Plate Bending," Proc. Conf. on Matrix Methods in Structural Mechanics, Wright-Patterson AFB, Ohio, 1965.

13. Bazeley, G. P., Cheung, Y. K., Irons, B. M. and Zienkiewicz, O. C., "Triangular Elements in Plate Bending - Conforming and Non-Conforming Solutions," Proc. Conf. on Matrix Methods in Structural Mechanics, Wright-Patterson AFB, Ohio, 1965.

14. Fraeijs de Veubeke, B., "Bending and Stretching of Plates - Special Models for Upper and Lower Bounds," Proc. Conf. on Matrix Methods in Structural Mechanics, Wright-Patterson AFB, Ohio, 1965.

15. Irons, B. M. and Draper, K. J., "Inadequacy of Nodal Connections in a Stiffness Solution for Plate Bending," AIAA Journal, Vol. 3, p. 965, 1965.

16. Bogner, F. K., Fox, R. L. and Schmit, L. A., "The Generation of Interelement, Compatible Stiffness and Mass Matrices by the Use of Interpolation Formulas," Proc. Conf. on Matrix Methods in Structural Mechanics, Wright-Patterson AFB, Ohio, 1965.

17. Argyris, J. H., "Continua and Discontinua," Proc. Conf. on Matrix Methods in Structural Mechanics, Wright-Patterson AFB, Ohio, 1965.

18. Felippa, C. A., Refined Finite Element Analysis of Linear and Nonlinear Two-Dimensional Structures, Ph.D. Dissertation, Department of Civil Engineering, University of California, Berkeley, California, 1966.

19. Bell, K., Analysis of Thin Plates in Bending Using Triangular Finite Elements, Institut for Statekk, Norges Tekniske Hogskole, Trondheim, Norway, 1968.

20. Irons, B. M., A Conforming Quartic Triangular Element for Plate Bending, Computer Program Report, Centre for Numerical Methods in Engineering, University of Wales, Swansea, Wales, 1968.

21. Greene, B. E., Jones, R. E., McLay, R. W. and Strome, D. R., "On the Application of Generalized Variational Principles in the Finite Element Method," AIAA Paper No. 68-290, AIAA/ASME 9th Structures, Structural Dynamics and Materials Conference, Palms Springs, Calif., 1968.

22. Mehrain, M., Finite Element Analysis of Skew Composite Girder Bridges, Ph.D. Dissertation, Dept. of Civil Engineering, Univ. of California, Berkeley, Calif., 1967.

23. Fraeijs de Veubeke, B., "An Equilibrium Model for Plate Bending," Int. Journal of Solids and Structures, Vol. 4, No. 2, 1968.

24. Morley, L. S. D., "A Triangular Equilibrium Element with Linearly Varying Bending Moments for Plate Bending Problems," Journal of the Royal Aero. Soc., Vol. 71, p. 715, 1967.

25. Herrmann, L. R., "A Bending Analysis for Plates," Proc. Conf. on Matrix Methods in Structural Mechanics, Wright-Patterson AFB, Ohio, 1965.

26. Herrmann, L. R., "Finite Element Bending Analysis of Plates," Proc. ASCE, EM-5, pp. 13-25, 1968.

27. Melosh, R. J., "A Flat Triangular Shell Element Stiffness Matrix," Proc. Conf. on Matrix Methods in Structural Mechanics, Wright-Patterson AFB, Ohio, 1965.

28. Martin, H. C., Stiffness Matrix for a Triangular Sandwich Element in Bending, Tech. Report 32-1158, Jet Propulsion Lab., Calif. Inst. of Tech., Pasadena, Calif., 1967.

29. Utku, S., "Stiffness Matrices for Thin Triangular Elements of Nonzero Gaussian Curvature," AIAA Journal, Vol. 5, No. 9, pp. 1659-1667, 1967.

30. Pian, T. H. H., "Element Stiffness Matrices for Boundary Compatibility and for Prescribed Boundary Stresses," Proc. Conf. on Matrix Methods in Structural Mechanics, Wright-Patterson AFB, Ohio, 1965.

31. Pian, T. H. H., "Finite Element Stiffness Methods by Different Variational Methods in Elasticity," AMS Symposium on Numerical Solution of Field Problems in Continuum Mechanics, Durham, N.C., April 1968.

32. Mikhlin, S. G., Variational Methods in Mathematical Physics, MacMillan Co., 1964 (translation of the 1957 Russian edition).

33. Kapur, K. K. and Hartz, B. J., "Stability of Thin Plates using the Finite Element Method," Proc. ASCE, Vol. 92, No. EM-2, 1966.

34. Clough, R. W. and Johnson, C. P., "A Finite Element Approximation for the Analysis of Thin Shells," Int. Journal of Solids and Structures, Vol. 4, No. 1, 1968.

APPENDIX

COMPATIBLE DISPLACEMENT FUNCTIONS

For subelement 3, Equation 17 gives $w^{(3)} = \hat{\phi}^{(3)}\, r$ where the displacement functions may be expressed: .

$$\hat{\phi}^{(3)} = \hat{\phi}^{(3)}_{w1}\ \hat{\phi}^{(3)}_{\theta x1}\hat{\phi}^{(3)}_{\theta y1}\ \hat{\phi}^{(3)}_{w2}\ \hat{\phi}^{(3)}_{\theta x2}\hat{\phi}^{(3)}_{\theta y2}\ \hat{\phi}^{(3)}_{w3}\ \hat{\phi}^{(3)}_{\theta x3}\ \hat{\phi}^{(3)}_{\theta y3}\ \hat{\phi}^{(3)}_{\theta 4}\ \hat{\phi}^{(3)}_{\theta 5}\hat{\phi}^{(3)}_{\theta 6}$$

in which (in terms of the dimensions and coordinates of the complete element):

$$\hat{\phi}^{(3)}_{w1} = \zeta_1^2(3-2\zeta_1) + 6\mu_3\zeta_1\zeta_2\zeta_3 + \zeta_3^2\left[3(\lambda_2-\mu_3)\zeta_1 + (2\mu_3-\lambda_2)\zeta_3 - 3\mu_3\zeta_2\right]$$

$$\hat{\phi}^{(3)}_{\theta x1} = \zeta_1^2(b_2\zeta_3 - b_3\zeta_2) + (b_1 - b_3\mu_3)\zeta_1\zeta_2\zeta_3 + \frac{1}{6}\zeta_3^2\left[3(b_2\lambda_2 + b_3\mu_3 - 2b_1)\zeta_1 + 3(b_3\mu_3 - b_1)\zeta_2 + (3b_1 - b_2\lambda_2 - 2b_3\mu_3)\zeta_3\right]$$

$$\hat{\phi}^{(3)}_{w2} = \zeta_2^2(3-2\zeta_2) + 6\lambda_3\zeta_1\zeta_2\zeta_3 + \zeta_3^2\left[3(\mu_1-\lambda_3)\zeta_2 + (2\lambda_3-\mu_1)\zeta_3 - 3\lambda_3\zeta_1\right]$$

$$\hat{\phi}^{(3)}_{\theta x2} = \zeta_2^2(b_3\zeta_1 - b_1\zeta_2) + (b_3\lambda_3 - b_2)\zeta_1\zeta_2\zeta_3 + \frac{1}{6}\zeta_3^2\left[3(2b_2 - b_3\lambda_3 - b_1\mu_1)\zeta_2 + 3(b_2 - b_3\lambda_3)\zeta_1 + (-3b_2 - b_1\mu_1 + 2b_3\lambda_3)\zeta_3\right]$$

$$\hat{\phi}^{(3)}_{w3} = \zeta_3^2\left[3(1+\mu_2)\zeta_1 + 3(1+\lambda_1)\zeta_2 + (1-\mu_2-\lambda_1)\zeta_3\right]$$

$$\hat{\phi}^{(3)}_{\theta x3} = \frac{1}{6}\zeta_3^2\left[3(3b_1 + b_2 + b_1\lambda_1)\zeta_2 + (b_2\mu_2 - b_1\lambda_1)\zeta_3 - 3(b_1 + 3b_2 + b_2\mu_2)\zeta_1\right]$$

$$\hat{\phi}^{(3)}_{\theta 4} = \frac{4A}{3L_3}\left[6\zeta_1\zeta_2\zeta_3 + \zeta_3^2(5\zeta_3 - 3)\right]$$

$$\hat{\phi}^{(3)}_{\theta 5} = \frac{4A}{3L_1}\left[\zeta_3^2(3\zeta_2\zeta_3)\right]$$

$$\hat{\phi}^{(3)}_{\theta 6} = \frac{4A}{3L_2}\left[\zeta_3^2(3\zeta_1 - \zeta_3)\right]$$

For $\hat{\phi}^{(3)}_{\theta yi}$ (i = 1,2,3) change all b's in $\hat{\phi}^{(3)}_{\theta xi}$ to a's.

Above expressions apply to subelement 3, where $\zeta_1 \geq \zeta_3$, $\zeta_2 \geq \zeta_3$

In subelements 1 (where $\zeta_2 \geq \zeta_1, \zeta_3 \geq \zeta_1$) and in subelement 2 (where $\zeta_3 \geq \zeta_2$, $\zeta_1 \geq \zeta_2$) permute cyclically all subscripts and superscripts (1-2-3 permutes to 2-3-1 and 4-5-6 to 5-6-4); for example: $\hat{\phi}^{(1)}_{wi} = \zeta_1^2\left[3(1+\mu_3)\zeta_2 + 3(1+\lambda_2)\zeta_3 + (1-\mu_3-\lambda_2)\zeta_1\right]$.